Analysis of Nighttime Drainage Winds in Boulder, Colorado during 1980

BRUCE W. HOOTMAN AND WILLIAM BLUMEN

Department of Astro-Geophysics, University of Colorado, Boulder, CO 80309

(Manuscript received 11 May 1982, in final form 9 March 1983)

ABSTRACT

Characteristics of nighttime drainage winds that occurred along the eastern slope of the Rocky Mountains around Boulder, Colorado during the calendar year 1980 are examined. The data used for this study were acquired from the Boulder Wind Network (BWN) and from the Boulder Atmospheric Observatory (BAO). Data were available almost continuously from BWN and less frequently from BAO. BAO is a 300 m tower, instrumented at eight levels, but only surface wind observations are obtained from BWN. However, the combination of BWN and BAO observations represents a relatively unique set of wind data for the examination of drainage flows.

Criteria for the identification of drainage winds are used to isolate events that are relatively free from external influences. Eighteen drainage wind events are identified, and some climatological features of the wind regime are established. In addition, the vertical structure of the flow associated with one event that reached the tower is examined in detail. Descriptions of the features of this flow and physical interpretations are presented. It is concluded, on the basis of this analysis, that observed features may be interpreted on the basis of the physical features contained in the model of Rao and Snodgrass (1981).

1. Introduction

Nighttime drainage winds have been observed in many parts of the world for several decades. Most of the observations of drainage winds are made with relatively low instrumented towers (Streten *et al.*, 1974) or with tethersondes (Manins and Sawford, 1979). These towers are useful for observing features that occur near the surface. Tethersondes are able to observe features further above the surface but have relatively long time resolutions (20–30 min) so they are only useful for observing relatively steady-state flows. Such observations are unsuitable for the examination of turbulent features, and observers are required to be at the site. This latter requirement restricts the number of events that can be observed. However, the data gathering systems used in the present study (both discussed in Section 2) represent a relatively unique set of data for the observation of drainage flows.

A study of drainage winds that occurred along the front range of the Rocky Mountains near Boulder, Colorado, during 1980 has been carried out. The purpose of this study is to examine an entire year of wind data and to isolate drainage flow events that are relatively unaffected by external influences. These data are suitable for determining the climatological distribution of drainage flows and for carrying out a detailed examination of the arrival of the flow at the Boulder Atmospheric Observatory tower east of Boulder. The turbulent nature of the leading edge of the flow could be delineated with high resolution (10 second average) wind and temperature data in addition to data obtained from an acoustic sounder located at the tower. Finally, the approximate steady state of the flow that tends to develop soon after passage of the leading edge is compared with the model results obtained by both Prandtl (1952) and Rao and Snodgrass (1981).

The observational data used in this study and the criteria used to identify drainage flows are presented in Section 2. The climatological information appears in Section 3. Observations of the leading edge or front of the flow are presented in Section 4. The steady state analysis is presented and compared with published model results in Section 5. A brief summary of the results obtained appear with concluding remarks in Section 6.

2. The region, the data, and the identification criteria

In this section the topography of the region, the data acquisition system, and the criteria for identifying drainage flows will be discussed.

a. The region

Examination of Figs. 1 and 2 shows that Boulder, Colorado (centered approximately at point C) is located near the foothills of the Rocky Mountains. The foothills are oriented approximately north–south, and the drainage flow forms on the slope of the foothills just to the west of Boulder. The slope has very complex terrain with numerous canyons, ridges, and mountain peaks. The fall line of the slope is roughly

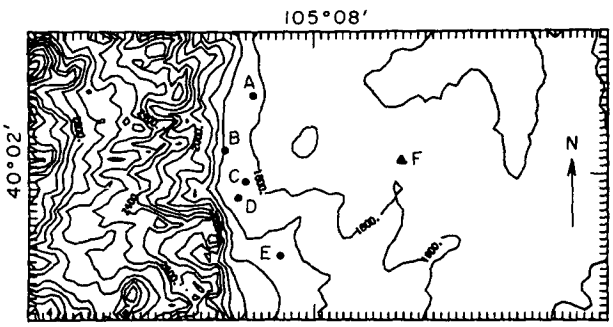

FIG. 1. Topography of the region showing the locations of BAO and BWN observation sites: (A) TBL, (B) NBL, (C) RB-3, (D) NBS, (E) MAR and (F) BAO. Contours are in 100 m intervals.

easterly with a grade of 5–7%. To the east of the slope there is an abrupt change from mountainous terrain to a relatively flat grassland valley. Boulder is located in Boulder Valley which is oriented roughly along a northeasterly line, with a grade of 1–2%.

b. The data

A part of the data set was collected by the Boulder Wind Network (BWN). BWN is operated by the Wave Propagation Laboratory of the National Oceanic and Atmospheric Administration (NOAA). The BWN consists of five sites located along the Front Range of the Rocky Mountains in the vicinity of Boulder. Fig. 1 shows the location of the five BWN sites. Continuous records of wind speed and wind direction measured by propeller-vane anemometers were available (except for periods of maintenance) during the calendar year 1980. All of the equipment at the different sites are the same. Each anemometer is located 7 m above the surface, except at RB-3 which is located atop the NOAA building at a height of 28 m above the surface. Observations are automatically recorded and the data stored on magnetic tape at one minute intervals. Twenty minute averages of the data are also stored in the computer memory.

The Boulder Atmospheric Observatory (BAO), also represents a principal data source. BAO is located about 25 km east of the foothills of the Rocky Mountains. BAO is a 300 m tower, instrumented at eight levels: 10, 22, 50, 100, 150, 200, 250 and 300 m. The instrumentation at each level consists of: a propeller-vane anemometer measuring horizontal wind speed and direction, a three-axis sonic anemometer measuring three orthogonal components of velocity, a quartz thermometer measuring temperature fluctuations, and a cooled-mirror hygrometer measuring dew-point temperature. Also, the atmospheric pressure at the surface is measured by five microbarographs. The sonic anemometers and the platinum wire thermometers are automatically sampled ten times per second by computer. The other instruments are sampled once per second, and all data are then stored on magnetic tape as ten second averages. Twenty minute averages of the data are stored in the computer memory. Certain data, including data from the sonic anemometers, are stored as "grab" samples; that is, one sampling from the ten second average period is stored on tape for that ten second period. Kaimal and Wolfe (1979) have provided a more detailed discussion of the BAO tower instrumentation.

Monostatic acoustic echo-sounders were in operation intermittently during 1980 at the BWN sites, RB-3 and TBL and at BAO (see Fig. 1 for location of these sites). The acoustic sounder radiates acoustic waves (with wavelength of about 0.2 m) which are scattered and returned to a detector. The scattering of acoustic waves by the atmosphere is represented by a model. The model shows that only variations of temperature (especially variations due to turbulence) can contribute to the backscatter of acoustic waves. Hence, the monostatic acoustic sounder records give information about the temperature structure and the turbulence structure. This is useful information for the study of drainage winds, which do exhibit turbulence. A more detailed discussion of the theory of acoustic wave scattering and the acoustic echo-sounder is given by Neff (1981) and Neff and Brown (1979).

The data set was augmented by three-hourly synoptic surface charts. Information about cloud cover, precipitation, synoptic scale pressure gradients, and frontal positions within Colorado and the surrounding area was obtained from these charts.

c. Identification of drainage flows

Since there are no observational sites on the slope, BWN site RB-3, near the foothills, was used to detect

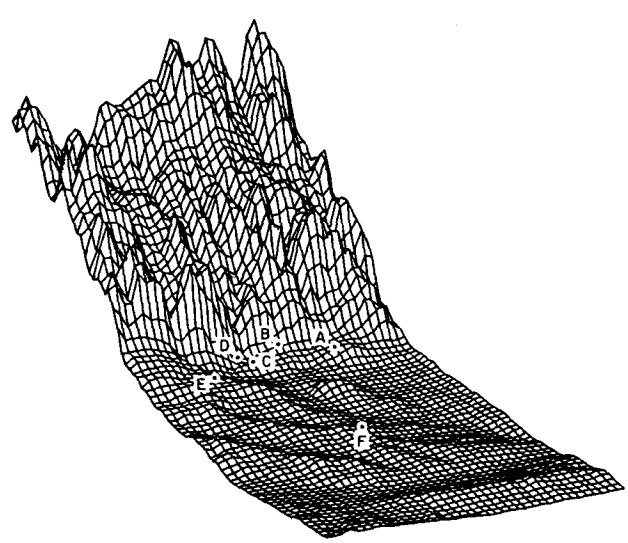

FIG. 2. Projection of the topography viewed from the southeast of RB-3. Locations of BAO and BWN observations are shown. Sites as in Fig. 1.

the onset of drainage winds. A primary requirement for the identification of a drainage flow is a change from easterly to westerly flow within two hours of sunset and persistence as a westerly wind through out the night. A restriction was placed on the peak speed of the flow: in order for the wind speed to be easily detected, no event with peak speed less than 2 m s^{-1} was considered. Also, to eliminate the possibility of relatively intense regional or synoptic scale downslope winds, no event with a peak speed greater than 8 m s^{-1} was considered. Twenty minute averaged wind speed and wind direction data from RB-3 were examined for the year 1980, and events that fit the above criteria were identified.

The question arises whether the flow observed is a drainage flow or is caused by other influences. For example, a frontal passage or a density current from a thunderstorm might show the same wind structure. In order to further eliminate large scale effects and examine only pure drainage flow events, additional restrictions were put on the synoptic scale situation in the vicinity. First, it was required that there be no fronts within 200 km of Boulder during the event. Second, it was required that the region be nearly cloudless during the flow. This requirement not only eliminated phenomena associated with convection and precipitation, but cloudless conditions are normally associated with enhanced radiative cooling from the surface. Third, it was required that synoptic pressure gradients be relatively weak, to further reduce the possibility of significant synoptic scale winds during periods of interest.

It must be noted here that these criteria for identifying drainage flows systematically exclude some drainage flow events. For example, drainage flows interrupted by a frontal passage or drainage flows that did not persist all night were excluded. Hence, the list of drainage wind events used in this study is an underestimate of the number of events that occurred during 1980. However, the drainage flow events that were considered appear to be relatively free from external influences. The exclusion of certain drainage wind events is not a serious limitation of the study, since only relatively pure drainage flow events are of interest here.

TABLE 1. Drainage wind events identified at RB-3 during 1980.

Date of event	Peak speed at RB-3 (28 m) (m s^{-1})	Peak speed at BAO (at height of maximum velocity)* (m s^{-1})
21 March	5	—
14 April	4	—
18 April	6	—
19 May	4	—
6 July	5	—
28 July	8	—
22 August	6	5
23 September	5	5
26 September	4	—
30 September	7	7
4 October	6	6
7 October	6	6
8 October	6	5
9 October	7	5
20 October	5	5
21 October	4	4
29 October	4	—
19 November	5	5

* Determined by cubic spline fit to the observations between the levels 10, 20, and 50 m.

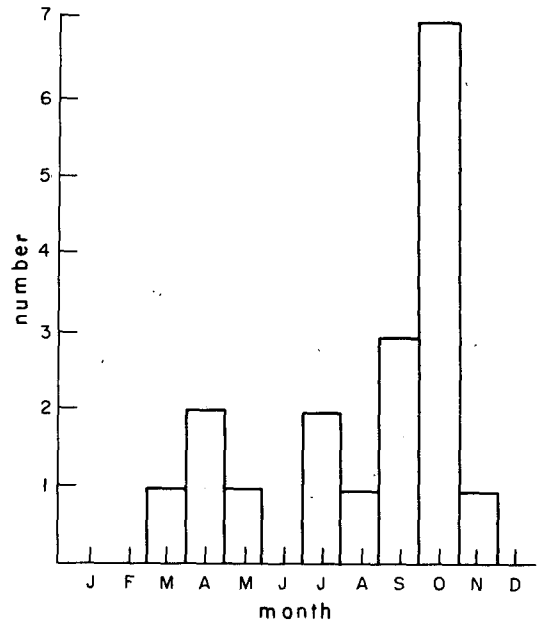

FIG. 3. Distribution by month of drainage winds events identified at RB-3 during 1980.

3. Climatology of drainage flows

Each drainage flow event is labeled by the day on which the flow existed after midnight. For example, if the flow began at 1800 MST 18 June 1980 and ended 0600 MST 19 June 1980, the flow event is labeled the event of 19 June 1980. The peak speed of the flow is defined as the maximum speed the flow attained throughout the flow. Table 1 lists the eighteen events that were identified at RB-3 during 1980 and the peak speed of each event. No drainage wind event had a peak speed of less than 4 m s^{-1}, and only one event had a peak speed of 8 m s^{-1}. The average peak speed is 5.4 m s^{-1}.

Figure 3 shows the distribution of drainage wind events observed at RB-3 during 1980. Most of the drainage winds were observed in September (17%), and October (39%). Other peaks in the distribution are April (11%) and July (11%). No drainage winds were observed in January, February, June, or December. Again it should be noted that the events identified

TABLE 2. Drainage flows at BAO and BWN sites.

Date of event	BAO	TBL	NBL	RB-3	NBS	MAR
18 April	N	Y	Y	Y	N	N
22 August	Y	N	Y	Y	N	N
23 September	Y	N	Y	Y	N	N
26 September	N	N	Y	Y	N	N
30 September	Y	Y	Y	Y	N	NA
4 October	Y	Y	Y	Y	N	NA
7 October	Y	Y	Y	Y	N	NA
8 October	Y	Y	Y	Y	N	NA
9 October	Y	Y	Y	Y	N	NA
20 October	Y	Y	Y	Y	N	NA
21 October	Y	Y	Y	Y	N	NA
19 November	Y	Y	Y	Y	N	NA

Y, drainage flow was observed; N, drainage flow was not observed; NA, data not available.

are not all the drainage winds that occurred in 1980, but they are the relatively clear-cut drainage wind events identified by the criteria described in Section 2.

This distribution may be related to the climate of the region during 1980. During summer months, the region is dominated by late afternoon and evening thundershowers, which would tend to disrupt drainage flows. During winter months, the frequent passage of winter storms tend to disrupt drainage flows. During the fall months, the days are usually warm, and the nights are usually clear and cold. The region is often dominated by slow moving high pressure systems that are conducive for the formation of drainage winds. Conditions that exist during spring months are similar to those existing during the fall, except that relatively more frontal passages tend to occur reducing the tendency for drainage flows to persist.

Table 2 lists the incidence of drainage winds at the other BWN sites when these events occurred at RB-3. For this analysis, only the 12 events that had BAO data were considered. Examination of Table 2 shows that drainage flow reached BAO about 83% of the time, and there seems to be a relationship between the peak speed at RB-3 and the flow reaching BAO (see Table 1). Ninety percent of the events that reached BAO had peak speeds at RB-3 of 5 m s^{-1} or larger, and 50% of the events that did not reach BAO had peak speeds at RB-3 less than 5 m s^{-1}. Presumably, the difference in peak speed at RB-3 is due to differences in radiative cooling at the ground, as has been predicted by Prandtl (1952) and Fleagle (1950). Hence, it may be speculated that differences in radiative cooling on the slope (and hence the differences in the peak speed) are responsible for whether or not the drainage flow reaches BAO. However, since the 18 April event did not reach BAO (6 m s^{-1} at RB-3), and the 21 October event did (4 m s^{-1} at RB-3), other processes acting on the flow may also contribute to the characteristic behavior.

Table 2 also shows that for every drainage wind event observed at RB-3, a drainage flow was observed at NBL, but no drainage wind was observed at NBS and MAR. Drainage wind events were observed at TBL about 69% of the time. Examination of the topography of the region (see Figs. 1 and 2) reveals that both RB-3 and NBL are located east of the month of Boulder Canyon so drainage winds could be expected to be observed at RB-3 and NBL. TBL is located near a smaller canyon that has more complex features than Boulder Canyon, so local topographic features could prevent the flow from being observed at TBL. West of MAR and NBS are some rather abrupt changes in topography (such as Green Mountain and South Boulder Peak) that presumably divert the flow away from NBS and MAR in some cases.

The observations presented in this section provide some insights into the effects of environmental conditions and topography on the characteristics of the drainage flow in this region. However, in view of the limited number of cases examined, the interpretations provided are as yet not conclusive.

4. Arrival of the drainage flow at BAO

The characteristic velocity and temperature fields of the flows that reached the BAO tower associated with the events of 30 September and 8 and 9 October are quite similar. The propagation characteristics for each case are displayed in Table 3. A light easterly flow of 1.0–1.5 m s^{-1} existed at low levels at BAO for

TABLE 3. Propagation characteristics of the drainage wind. BAO is located 21.7 km west of RB3.

Date of event	Passage at RB3 (MST)*	Passage at BAO (MST)**	Propagation speed (m s^{-1})	One-hour averaged west wind (m s^{-1})***		
				RB3 (28 m)	BAO (10 m)	BAO (22 m)
30 September	1735	1850	4.8	5.1	3.4	4.7
8 October	1725	1939	2.7	3.9	3.0	4.2
9 October	1726	1910	3.5	4.4	2.4	3.2

* The wind shifts from easterly to westerly occurred over a 10–20 minute period. Mid-time values are presented.

** The passage for the 30 September event was not abrupt, occurring over an approximate 10 minute period. The remaining two passages occurred abruptly.

*** Approximate steady-state values after the frontal passage.

the two October events prior to the arrival of the drainage flow. However, for the event of 30 September a light westerly flow existed at BAO before the drainage flow arrived. Flow speeds were about 0.5 m s^{-1} below 100 m but increased to about 1.5 m s^{-1} above 100 m. This latter feature probably accounts for the more rapid westerly propagation speed, displayed in Table 3, compared to the propagation speeds associated with the October events.

The event of 9 October will be examined in detail. This case is representative of the other two cases and, fortunately, acoustic sounder data were available for the duration of the flow, although BAO data were only available up to 2040 MST. Composites of the relatively steady-state flow of the three events will be presented in Section 5.

Ten-second averaged data were used to derive thirty-second, one-minute, and four-minute averages. These data were suitable for a detailed examination of the arrival of the flow at BAO. A standard cartesian coordinate system is used, with x, y, and z directed eastward, northward and upward, respectively. It must be remembered that the tower is not located on the eastward facing slope where the downslope flow formed but is located on relatively flat plain ~25 km east of the foothills.

Fig. 4 shows the vertical structure of the west wind (along the fall line of the slope) exhibited by thirty-second averaged data at 1910, 1911 and 1912 MST 9 October. The vertical structure of the south wind (perpendicular to the fall line of the slope) for the same period is shown in Fig. 5. Wind velocities were measured by the propeller-vane anemometers and checked against the sonic anemometers. Comparisons between the two measurements of velocity assured accuracy and consistency of the observations. Fig. 6 shows the vertical structure of temperature for the same times. Temperatures were measured by quartz thermometers at each level. The uncertainties of the velocity and temperature measurements are 0.1 m s^{-1} and 0.1 K, respectively.

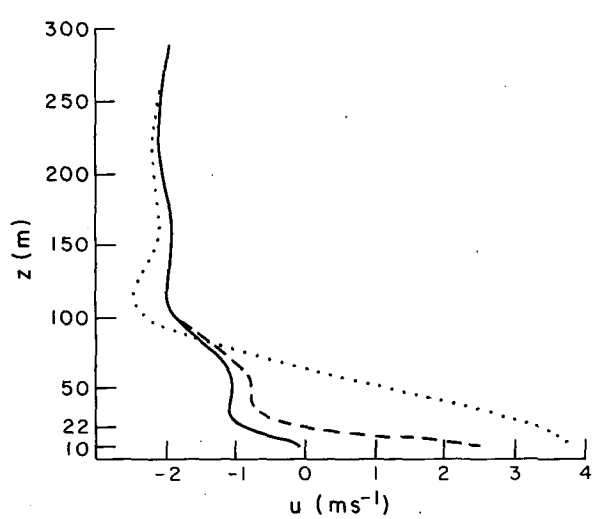

FIG. 4. West wind (u) for the event of 9 October, showing the arrival of the drainage flow for the times 1910 (solid line), 1911 (dashed line), and 1912 MST (dotted line). The data are averaged over 30 seconds.

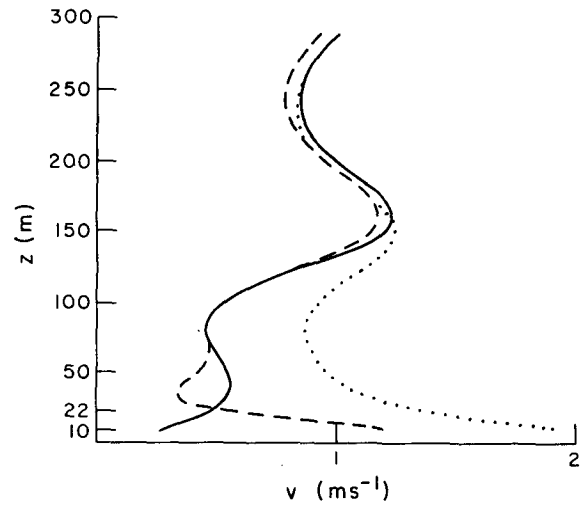

FIG. 5. As in Fig. 4 but for south wind (v).

The drainage flow had not quite reached the tower at 1910 MST. At 1910 MST, the west wind is relatively calm at the 10 m level and increases with height until 100 m where it is easterly ~1.9 m s^{-1}. Above 100 m the flow is relatively constant with height. At the same time the south wind is nearly calm at 10 m and increases to southerly ~1.2 m s^{-1}. Above 100 m the wind vector is southeasterly and nearly constant in direction. The temperature structure at 1910 MST shows the nocturnal inversion (sunset is around 1730 MST) that formed in the layer nearest the surface (10 m and 22 m). From 100 m to 300 m the lapse rate is nearly constant with a value of 8 K km^{-1}.

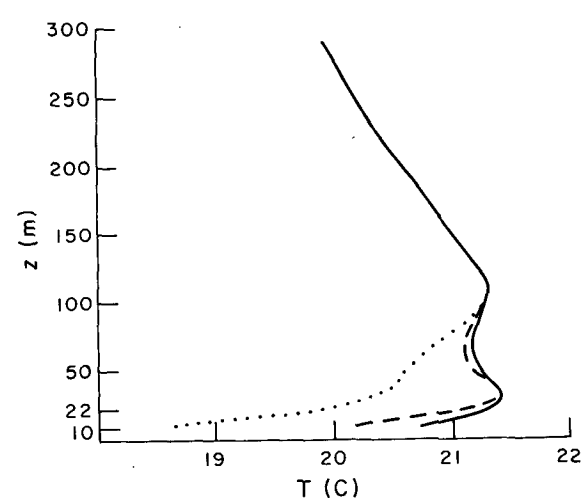

FIG. 6. As in Fig. 4 but for temperature (T).

This 300 m boundary layer is statically stable at all levels.

At 1911 MST, the westerly flow at 10 m increases to ~2.6 m s^{-1} and at 22 m the direction shifts from easterly to westerly. Again, the profile above 100 m is unaffected. Fig. 5 for 1911 MST shows that the southerly component of velocity continues to increase at the 10 and 22 m levels. Above 100 m profile is unaffected. Fig. 6 shows a temperature drop of 0.4 K at the 10 m level and 0.2 K at the 22 m level. There is still no change above 100 m.

By 1912 MST changes in the wind velocity have progressed up to about 150 m, with relatively little change noted above this level. The maximum speeds are at 10 m, where the westerly wind has increased to 3.9 m s^{-1} and the southerly wind to 1.8 m s^{-1}. Significant decreases in temperature have also occurred, but these are confined to the lowest 100 m.

The relatively sudden drop in temperature is more evident in Fig. 7. A relatively slight linear cooling rate at the 10 m level exists before 1910 MST with a cooling rate at 10 m ~3.5 K hr^{-1}. Before the arrival of the flow (1910 MST), the cooling of the lower layers (up to 100 m) is most likely due to radiational loss. The linear cooling rate is also observed up to 100 m,

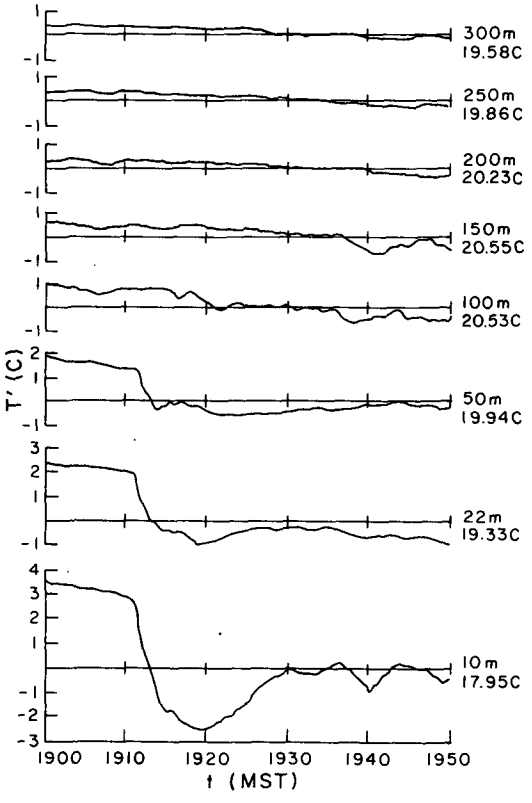

FIG. 7. Time series of temperature deviation (T') from the one-hour averaged temperature at eight levels for the event of 9 October. Height of the level and mean temperature are given at the right of each plot.

but above 100 m the temperature is nearly constant. About 1910 MST the 10 m level temperature begins to fall and by 1920 MST the temperature has dropped by ~5.5 K. A temperature drop is also observed at the 22 and 50 m levels, but the drop at 22 m is delayed by about a minute and at 50 m by about two minutes. This behavior is associated with the fact that the leading edge of the flow slopes upstream. The period between about 1920 and 1930 MST is characterized by temperature increases at 10, 22 and 50 m. This period is then followed by marked fluctuations in temperature at 10 m, but this tendency is not as pronounced at the upper levels. However, small fluctuations in the temperature at 100 m and slightly later at 150 m appear to indicate that the influence of the drainage flow has extended to these levels.

The monostatic acoustic sounder record is shown in Fig. 8. The monostatic acoustic sounder detects temperature structure due to turbulence much more efficiently than other scales of temperature structure; hence, Fig. 8 shows the time evolution of the turbulence at the tower. No echoes were recorded before 1910 MST near the surface, but ~1910 MST turbulence is observed very near the surface. For the next 20 minutes the depth of the turbulent layer increases until the layer is nearly 200 m in depth. Between 1910 and 1920 MST the echoes are very strong, after 1920 MST they weaken. There appears to be a very well defined boundary between the turbulent region embedded in the leading edge of the flow and the quiescent region ahead of it. This observation is supported by the velocity and temperature profiles examined above. Moreover, the flow in the lower layers seems to be uncoupled from the upper region.

The turbulent nature of the flow may be further delineated by means of the 10-second grab samples from the sonic anemometer data. Fig. 9 shows records of uw as functions of time for the eight levels, where both u and w represent deviations from 30-minute average values. A significant increase in the magnitude of the fluctuation of uw appears at the 10 m level at ~1910 MST, when the flow arrives. This "burst of turbulence" lasts for about 10 minutes, corresponding to the region of strong turbulence observed in the acoustic sounder record. Large uw fluctuations at the 22 and 50 m levels begin shortly before the actual arrival of the flow at these levels. These fluctuations represent a precursor ahead of the leading edge of the front at the 10 m level. After 1915 MST the fluctuations of uw decrease (at 10, 22 and 50 m), and do not return to the levels observed before the arrival of the flow. The region above 150 m remains relatively quiescent during the low level passage.

Fig. 10 shows the time series of w^2 for the eight levels of the tower. Before 1910 MST, w^2 shows the same non-turbulent behavior as uw, and during passage of the leading edge the fluctuations in w^2 are also

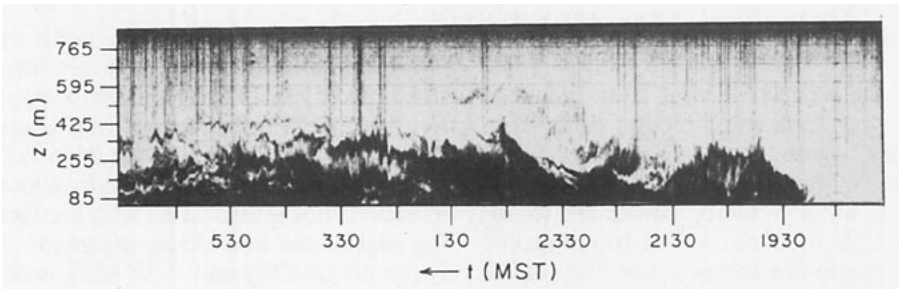

FIG. 8. Acoustic sounder record for the event of 9 October showing the arrival of the drainage flow. Black indicates an echo at that level, while white indicates no echo.

observed to increase in magnitude. However, just after 1910 MST, Fig. 10 shows that increased fluctuations in w^2 occur at all levels associated with the passage of the leading edge. Although the air is relatively non-turbulent at the upper levels, as observed by the acoustic sounder record (Fig. 8) and the time series of uw (Fig. 9), the observations shown in Fig. 10 appear to indicate that the advancing cold air initiates upslope motion of the relatively warmer ambient air along its leading edge or front.

In summary, several features associated with the arrival of the drainage flow at the tower have been delineated. The passage of the leading edge of the flow is a distinctly observed feature. After passage of the leading edge, the air becomes more turbulent than the ambient air outside the flow, but the leading edge is associated with the coldest and most turbulent part of the drainage flow. These features are revealed in the acoustic sounder record, which shows that the leading edge has a definite boundary between the flow and the ambient air both above and in front of the flow. The acoustic sounder record after 1930 MST (Fig. 8) also shows relatively less turbulence within the drainage flow in the region away from the leading edge. In addition, the sloping frontal surface observed in the acoustic sounder record confirms that the flow arrives at the lower levels before it arrives at upper levels as indicated by the wind and temperature behavior (see Figs. 4, 5 and 6).

A southerly wind component is also associated with the arrival at the tower. This is a typical characteristic of the flow at BAO. The BAO tower is located on the southern edge of Boulder Valley (see Fig. 1). The valley is oriented northeasterly. The southerly flow at the tower below 50 m may be explained as a southerly turning of the flow guided by the shape of the valley.

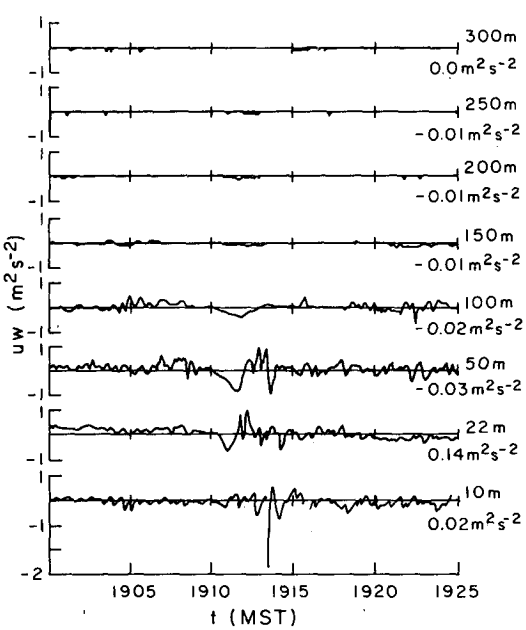

FIG. 9. As in Fig. 7, but for time series of uw.

5. Analysis of the flow behind the leading edge

For present purposes, the approximate steady state is defined as follows: the flow is said to be in approximate steady state if the shape of the velocity profile does not change significantly and the velocity maximum does not change significantly (~10%), in height or magnitude over two or more 20-minute average periods. Three events were examined in this phase of the study: the events of 30 September, 8 October and 9 October. Each of these events are relatively similar in terms of the profiles of heat flux, momentum flux, temperature, and velocity as indicated by the composites of these data displayed in Figs. 11–14. Because of the similar behavior of the three events, only one representative case will be discussed in detail, the event of 9 October 1980.

The underlying assumption of this analysis is that the drainage flow essentially maintains its vertical structure as it moves out onto the plains. The drainage flow may then be compared to theories of the drainage wind presented by Prandtl (1952) and Rao and Snodgrass (1981). This assumption appears to be reasonable, since the peak velocities did not change very much after travel from RB-3 to BAO (see Table 1). For each of the events examined, an approximate steady state was reached within ~30–90 minutes after the arrival of the flow at BAO.

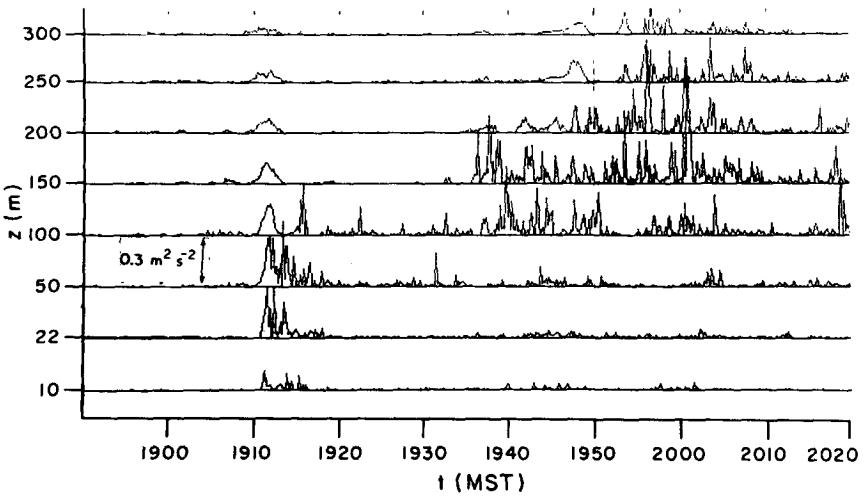

FIG. 10. As in Fig. 7 but for time series of w^2. The scale of each plot is 0.3 m^2 s^{-2}.

Fig. 11 shows the one-hour averaged west wind at BAO for the event of 9 October for the period beginning at 1940 MST. The data points between the instrumented levels were interpolated by a cubic spline routine [see Pennington (1965)]. Examination of the spline fit to analytic profiles resembling the observed drainage wind at BAO (such as Prandtl's solution) showed that the spline fit could identify the height of the velocity maximum to within 1 m. Consequently, the height of the velocity maximum of the observed drainage flow could then be pinpointed more accurately. The maximum velocity and the height of the maximum velocity completely specify Prandtl's solution. Hence the constant eddy exchange coefficients of heat and momentum are also specified in this solution. Fig. 11 also shows Prandtl's solution fit to the data, where the maximum velocity and height of maximum velocity were determined from the spline fit to the data. There are a number of features of the observed velocity profile to be noted. The velocity of the flow increases with height to ~41 m. (It is presumed that the velocity vanishes at the ground.) At about 41 m the velocity reaches a maximum of about 3.6 m s^{-1}. Above 41 m the velocity decreases then becomes easterly, reaching 1.5 m s^{-1} at 300 m. The relatively higher magnitudes, associated with the composite profile, primarily reflect the ambient westerly flow that accompanies the 30 September event. The affect of this ambient current on propagation speed of the front of the drainage current was noted in Section 4.

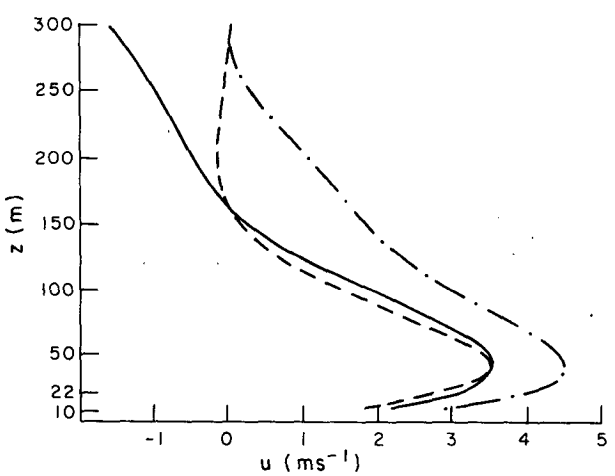

FIG. 11. West wind u for the event of 9 October (solid), averaged over one-hour (1940–2040 MST), Prandtl's solution fit to the data (dashed), and composite of the three events (dashed–dot).

Comparison between Prandtl's solution and the observed profile (Fig. 11) shows that the general shape of the flow is preserved below the 200 m level. The deviation above is not significant since the region above 200 m is undoubtedly outside the layer dominated by the drainage flow.

Rao and Snodgrass (1981; Fig. 4) introduced the height dependence of the eddy diffusivities into a drainage flow model. Their results show that the eddy diffusivities are larger away from the surface, and are smaller close to the surface than the constant value of Prandtl's model. As a consequence, eddy diffusion of momentum away from the velocity maximum is more efficient in Rao and Snodgrass' model. This process results in larger velocities, both above and below the velocity maximum, than those determined in Prandtl's model. Consequently, Rao and Snodgrass' model results are consistent with the observed features shown in Fig. 11. Then the differences between the present observations and Prandtl's solution may be explained in light of the physical processes contained in Rao and Snodgrass' model: the mixing

lengths, which are relatively small near the surface, are further compressed by the large stable stratification that exists (see Fig. 13); aloft a reduced stratification enhances larger mixing lengths.

The profile of the average vertical flux of westerly momentum per unit mass $\overline{uw}$, for the event of 9 October, is shown in Fig. 12. The observations show that westerly momentum is transferred both upward and downward away from the level of the velocity maximum. The downward flux offsets the loss by friction at the ground. Momentum also converges above the 150 m level because momentum transfer is not efficient in this relatively quiescent region (see also Fig. 9).

Fig. 13 shows the vertical structure of the average temperature for the event of 9 October. There is a surface based temperature inversion up to ~100 m, presumably associated with radiational cooling. The inversion is also strengthened by the advection of colder air at low levels in conjunction with the drainage flow. Above, the temperature decreases with height, with a mean lapse rate of 4.1 K km^{-1}. The entire layer from the surface to the 300 m level is statically stable. Figure 13 also shows Prandtl's solution fit to the average temperature profile. The relatively warmer temperatures that are observed above a surface layer ($z \geq 10$ m) and below the top of the inversion reflect the process of downward heat transfer that is revealed in the vertical distribution of $\overline{wT}$, displayed in Fig. 14. Alternatively, upward flux of cool air is inhibited by the large stable stratification that exists. Similar features appear in Rao and Snodgrass' results (Figs. 3 and 4). However, the observed temperatures and those in Rao and Snodgrass' model results tend to become cooler than Prandtl's values just above the surface. This latter feature is a consequence of the finite heat diffusivity in Prandtl's model compared to the vanishingly small values in the surface layer of Rao and Snodgrass' model. The observed heat transfer $\overline{wT}$ also vanishes at the ground, but positive values exist in a shallow layer just above the ground. This latter feature also exists in the data for the event of 30 September, but the heat flux is essentially zero at 10 m during the averaging period of the 8 October event.

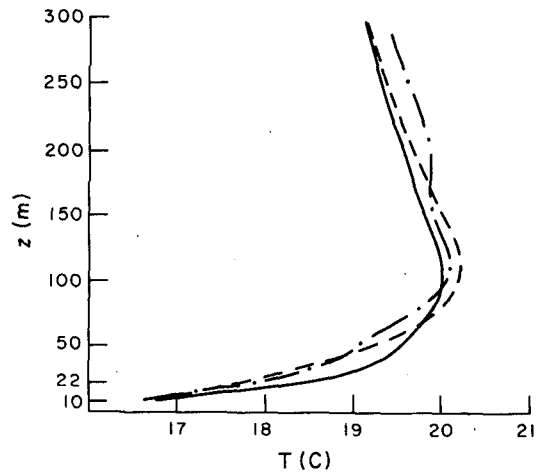

FIG. 13. As in Fig. 11 except for temperature T.

The ratio of eddy diffusivity of heat (K_h) to eddy diffusivity of momentum (K_m) is independent of the slope angle in Prandtl's solution. Consequently a comparison may be made between this ratio determined from Prandtl's solution, fit to the average data of the 9 October event, and the ratio determined by

$$\frac{K_h}{K_m} = \frac{\overline{wT}(\partial\bar{T}/\partial z)^{-1}}{\overline{uw}(\partial\bar{u}/\partial z)^{-1}}. \quad (1)$$

The value $K_h/K_m = 2.3$, calculated from Prandtl's solution, is a constant. The ratios, calculated directly from the data (see Figs. 11–14), and expressed as layer averages, are:

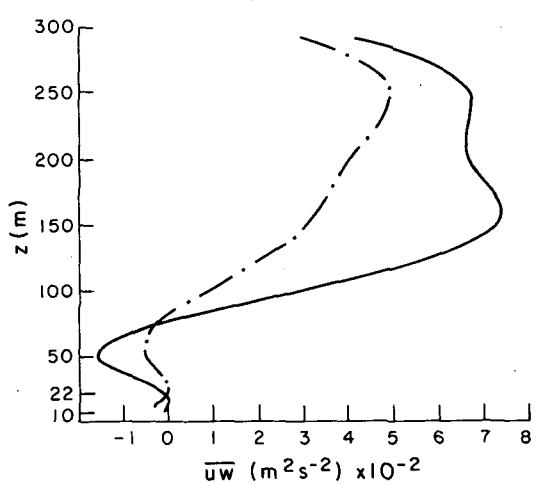

FIG. 12. Distribution of $\overline{uw}$ (one-hour average) for the event of 9 October (solid) and composite (dashed–dot).

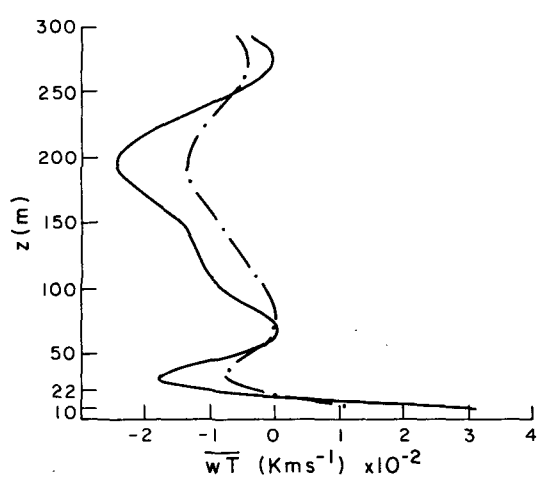

FIG. 14. As in Fig. 12 except for $\overline{wT}$.

$$\left.\begin{aligned}\left.\frac{K_h}{K_m}\right|_{0\text{–}50\text{m}} &= \frac{-4.2\times10^{-2}}{-7.6\times10^{-2}} = 0.55\\ \left.\frac{K_h}{K_m}\right|_{50\text{–}100\text{m}} &= \frac{-29.5\times10^{-2}}{-6.1\times10^{-2}} = 4.84\end{aligned}\right\}.$$

The seven-fold increase in the layer-averaged value of K_h is associated with the relatively small temperature lapse rate in the 50–100 m layer. The average for the 0–100 m layer is $K_h/K_m = 2.7$. This relatively good agreement with the value of 2.3, determined from Prandtl's solution is not at variance with the assumption that the drainage flow maintains its vertical structure, at least over the 25 km distance between the foothills and BAO.

6. Concluding remarks

An identification and analysis of drainage winds observed near Boulder, Colorado, during 1980 has been presented. Most drainage wind events were observed in September (17%) and October (39%) in association with the relatively frequent presence of anticyclones with weak pressure gradients. In addition, the drainage winds formed possess significant inertia since the flow reached BAO about 83% of the time that it was observed at RB-3. There is evidence that the peak speed of the flow at RB-3 has an effect on whether the flow reaches BAO, but the evidence is not conclusive.

The observations and the acoustic sounder record show the leading edge of the flow has a relatively well defined boundary that slopes upstream. In addition, the observed drainage flow is more turbulent than the ambient air above the flow, and the leading edge of the flow is the coldest and most turbulent part of the flow. As the flow arrives, ambient air is forced to move upslope. This effect is observed as a precursor to the arrival of the flow. These observations are in essential agreement with both field observations and laboratory simulations of, so-called, density or gravity currents over level boundaries. Simpson (1982) has shown that the development of such currents may be traced to drainage flows and thunderstorm outflows, among others.

Within about an hour after passage of the leading edge, a relatively steady-state flow becomes established. Further, the properties of this observed steady state flow tend to support the variable eddy diffusivity model predictions presented by Rao and Snodgrass. Consequently, the mixing lengths in the observed flows are smaller near the surface and larger aloft than the constant mixing length that characterizes Prandtl's classical model.

Retardation of the drainage flow due to interfacial entrainment of ambient air should be an important consideration in model development that takes account of three-dimensional dynamical processes, as noted by Manins and Sawford (1979). Unfortunately, this effect cannot be evaluated with confidence using data from a single tower unless very stringent constraints are adopted. Perhaps the most significant unknown is the lateral divergence associated with the flow as it moves eastward.

Acknowledgments. Financial support for this investigation was supplied by the National Oceanic and Atmospheric Administration under Grant NA 81 RAD00011. The authors wish to thank the staffs of the Boulder Atmospheric Observatory and the Wave Propagation Laboratory for their patience and helpfulness with many questions, problems, and requests. Special thanks to C. Kaimal, J. Gaynor, and A. Bedard for their advice and help with the BAO and BWN data; to W. Neff and C. King who supplied the acoustic sounder records, and to J. Birtwhistle and N. Dirks who supplied data at every request.

REFERENCES

Fleagle, R. G., 1950: A theory of air drainage. *J. Meteor.*, **7**, 227–232.

Kaimal, J. C., and D. E. Wolfe, 1979: BAO site, tower instrumentation, and Phoenix operations, Chap. 2 in Project Phoenix: The September 1978 field operation, W. H. Hooke, Ed. NOAA/NCAR Boulder Atmospheric Observatory Rep. No. 1, 16–32.

Manins, P. C., and B. L. Sawford, 1979: Katabatic winds: A field case study. *Quart. J. Roy. Meteor. Soc.*, **105**, 1011–1025.

Neff, W. D., 1981: An observational and numerical study of the atmospheric boundary-layer overlying the east Antarctic ice sheet. NOAA Technical Memorandum ERL WPL-67, 272.

——, and E. H. Brown, 1979: Acoustic echo sounder operations during Phoenix, Chap. 14 in Project Phoenix: The September 1978 Atmospheric Observatory Rep. No. 1, 157–175.

Pennington, R. H., 1965: *Introductory Computer Methods and Numerical Analysis.* The Macmillan Company, 452 pp.

Prandtl, L., 1952: *Essentials of Fluid Dynamics.* Blackie and Son Ltd., London and Glasgow, 452 pp.

Rao, K. S., and H. F. Snodgrass, 1981: A nonstationary nocturnal drainage flow model. *Bound.-Layer Meteor.*, **20**, 309–320.

Simpson, J. E., 1982: Gravity currents in the laboratory, atmosphere and ocean. *Annual Review of Fluid Mechanics,* Vol. 14, 213–234.

Streten, N. A., N. Ishikawa and G. Wendler, 1974: Some observations of the local wind regime on an Alaskan glacier. *Arch. Meteor. Geophys. Bioklim.*, **B22**, 337–350.